Wissenschaftliche Gesellschaft Lasertechnik e.V.

Lasers in Manufacturing Conference 2017

Layer-selective laser-lift off and removal mechanism in a TCO/Si thin film system by nano- to femtosecond pulses

S. Krause[a,b,*], P. Miclea[a,c], K. Kaufmann[a,b], C. Hagendorf[a], N. M. Bulgakova[d]

[a] *Fraunhofer Center for Silicon Photovoltaics CSP, Otto-Eißfeldt-Straße 12, 06120 Halle, Germany*
[b] *Anhalt University of Applied Sciences, Bernburger Straße 55, 06366 Köthen, Germany*
[c] *Martin Luther University of Halle-Wittenberg, µMD Group - Institute of Physics, Heinrich-Damerow-Str. 4, 06120 Halle, Germany*
[d] *HiLASE Centre, Institute of Physics ASCR, Za Radnicí 828, 25241 Dolní Břežany, Czech Republic*

Abstract

Narrow craters and trenches have been scribed into Si/TCO thin film systems on glass by selective laser lift-off using nano-, pico- and femtosecond pulses of ~ 0.5 µm wavelength. A high-resolution microstructural material investigation shows a significant reduction of heat affected zone (HAZ) by changing from ns to ps and fs pulse durations. Thus, ablation efficiency and selectivity of ps- and fs-lift-off thin film processing in comparison to thermal ablation by ns pulses is strongly increased. Difference in film removal mechanisms depending on pulse duration is discussed based on multi-layer thermal modeling of the laser-induced spatio-temporal temperature fields. For ultrashort laser pulses, a continuum model has been applied, aimed at describing the dynamics of electronic excitation, heating, and melting at TCO/Si interface region under femto- and picosecond laser irradiation.

Keywords: Laser lift-off; ultra-short pulses; transparent conductive oxide; Si micro processing; laser-interaction modelling

1. Introduction

Laser lift-off processes are used for layer-selective micro-structuring of various thin film systems on rigid or flexible substrates ranging from display technology, LED devices to organic and inorganic PV thin films. Femtosecond (fs) laser lift-off processes are known to be initiated by ultrafast melting of interfacial layers in thin film systems. A suitable laser wavelength allows pulse propagation through substrate, here glass and transparent conductive oxide layers (TCO), towards the absorbing interface (here amorphous silicon) in a typical superstrate thin film configuration. This ablation technique is called "confined" laser ablation if the

* *E-mail address:* s.krause@emw.hs-anhalt.de .

energy is mainly absorbed at an interface of two solid layers and was comprehensively investigated by several groups [1-3] on different thin film systems. By time-resolved microscopy, Domke et al. [4] studied ablation stages on film side and substrate side of the irradiated Mo/glass systems and built up an understanding of thin film ablation considering laser pulse penetration depth and film thickness. They found an efficiency advantage for confined laser ablation (substrate side irradiation) compared to direct laser ablation by a factor of 10 for 10 ps laser pulses. In addition, the ablation of intact disks of removed material was observed, if the film thickness exceeds a critical value larger than the optical penetration depth.

The goal of this study is to investigate microstructural properties of such ablated disk material and produced laser craters, as well as pulse duration dependence of the removal mechanisms from short (nanosecond) to ultrashort (femtosecond) regimes. The thickness of laser-affected zones and material modifications are measured by high-resolution microstructural techniques. Ns-processing results are complemented by multi-layer thermal modeling of the laser-induced evolution of spatiotemporal temperature fields. For ultrashort laser-interaction, a continuum model is under development, aimed at describing the dynamics of electronic excitation, heating, and melting at TCO/Si interface region under picosecond and fs laser irradiation. Differences in film removal mechanisms depending on pulse duration are discussed by considering optical, geometrical, thermal and mechanical properties of the layers.

2. Experimental

In this study, we investigated nano-, pico-, and femtosecond laser ablation (ns, ps, and fs respectively) of a thin film Si/TCO/glass layer system. The sample stack consists of ~ 800 nm microcrystalline (µc-Si) and ~ 250 nm thick amorphous silicon (a-Si) deposited on a ~ 600-700 nm textured Al-doped zinc oxide (AZO) layer on soda-lime float glass sheets of ~ 3 mm thickness (see Fig. 1, left). In addition, a thin buffer layer of ~ 100 nm is deposited between the glass substrate and the AZO layer. The laser processing was performed through the glass using short and ultra-short pulses of a ns Nd:YVO4 (λ = 532 nm; $\Delta\tau$ = 10 ns; P_{max} = 15 W; f_{max} = 50 kHz), a ps Nd:YVO4 (λ = 532 nm; $\Delta\tau$ = 10 ps; P_{max} = 25 W; f_{max} = 1 MHz) and a fs Yb:KGW laser systems (λ = 515 nm; $\Delta\tau$ = 200 fs; P_{max} = 3 W; f_{max} = 600 kHz). For focusing and positioning, f-theta lenses with focal lengths of about 160 mm (or 100 nm) were used in combination with a xyz-scanner.

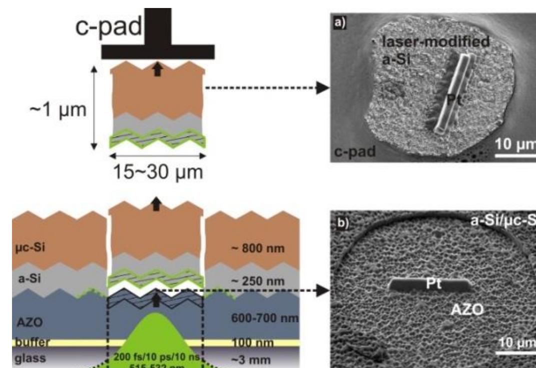

Fig. 1. Schematic image of the laser-treated thin film stack and the capture method by positioning of a carbon-pad behind the sample. SEM images of the opened a) captured thin film disk and b) laser crater after laser lift-off processing.

After laser processing, the ablation spots and collected ablated material were characterized using laser scanning microscopy (images acquired with a Keyence VK-X100) as well as scanning electron microscopy (SEM) and transmission electron microscopy (TEM) after preparation of TEM lamellas (Fig. 1, right). TCO and Si material phases are identified by energy dispersive x-ray (EDX) analysis in TEM measurements. Raman

measurements were also performed to locally analyze crystalline and amorphous phases within the HAZ of laser craters and on the ablated material with a S&I triple micro-Raman spectrometer. Raman scattering was measured in backscattering geometry using a confocal microscope after excitation with 488 nm irradiation.

3. Theoretical

The modeling of laser heating of the thin film stack in the regimes of laser treating utilized in this study has also been performed for ns, ps, and fs laser pulses to gain an insight into driving mechanisms of ablation.

3.1. Nanosecond laser pulses

At ns laser pulses when electron-lattice coupling time (for silicon it is ~several ps depending on excitation conditions) is much smaller than pulse duration, the interaction of laser light with silicon can be considered in the frames of the thermal model [14]. In this study, we use the model [15] developed for investigations of laser scribing conditions for multilayer photovoltaic materials. The time-dependent temperature distribution in the film stack is simulated using the heat-flow equation written for each film in the following form:

$$\left(c_p\rho + L_m\delta(T - T_m)\right)\frac{\partial T}{\partial t} = \frac{\partial}{\partial x}\lambda\frac{\partial T}{\partial x} + \Sigma(x,t), \tag{1}$$

where ρ, c_p, and λ are the material density, the heat capacity, and the thermal conductivity respectively. The term $L_m\delta(T - T_m)$ (T_m and L_m are the temperature and enthalpy of melting) is introduced for a case of melting of the corresponding layer, allowing to follow the dynamics of the liquid–solid interface. In our case (scheme in Fig. 1), the source term of the laser energy can be written in a simplified form as verified in simulations:

$$\Sigma(x,t) = (1 - R_{\mathrm{AZO}})(1 - R_{\mathrm{a-Si}})\alpha_{\mathrm{a-Si}} I(t)\exp\left(-\alpha_{\mathrm{a-Si}}(x - \Delta x_{\mathrm{glass}} - \Delta x_{\mathrm{AZO}})\right). \tag{2}$$

Here $I(t)$ is the Gaussian shape of the laser intensity; R_{AZO} and $R_{\mathrm{a\text{-}Si}}$ are respectively the reflection coefficients of the AZO and amorphous silicon films; $\Delta x_{\mathrm{glass}}$ and Δx_{AZO} are the thicknesses of glass and AZO layers; $\alpha_{\mathrm{a\text{-}Si}}$ is the absorption coefficient of amorphous silicon. Thus, laser radiation is absorbed only in the a-Si layer and the absorbed energy is transferred to other films in stack by thermal conduction. This is simulated via appropriate boundary conditions which is the equality of the heat flows in the two adjacent materials. As an example, for the interface between the AZO and a-Si films the boundary condition reads as:

$$\lambda_{\mathrm{AZO}}\left.\frac{\partial T}{\partial x}\right|_{\mathrm{AZO}} = \lambda_{\mathrm{a-Si}}\left.\frac{\partial T}{\partial x}\right|_{\mathrm{a-Si}}. \tag{3}$$

The glass layer was taken thick enough to consider T = 300 K on its free boundary through which the laser light is propagating to the film stack. At the remote boundary µc-Si/air, the heat flow absence was assumed.

The thermophysical properties of glass, a-Si and µc-Si were taken as in work [15]. For AZO film, the following properties were taken: ρ = 5.7 g/cm^3; T_m = 2248 K; L_m = 9.7×10^5 J/kg; c_p = 494 J/(kg K); λ = 20 W/(m K); R_{AZO} = 0.14. The complex refractive index of a-Si for the used green light is $n + ik = 4.49 + i0.97$.

3.2. Picosecond and femtosecond laser pulses

For ultrashort laser pulses when pulse duration is shorter than or comparable with the characteristic electron-phonon coupling time, the two-temperature model is applied to simulate laser energy absorption and sample heating dynamics. For a-Si-film where laser light is absorbed, the heat flow equations are written separately for free electrons generated by the laser pulse and the lattice while in the other films the equations have the form (1) accounting for the absence of free electrons in these layers. The two-temperature model reads as [16]:

$$C_e \frac{\partial T_e}{\partial t} = \frac{\partial}{\partial x} \lambda_e \frac{\partial T_e}{\partial x} - g(T_e - T) + \Sigma(x,t), \tag{4}$$

$$\left(c_p \rho + L_m \delta(T - T_m)\right) \frac{\partial T}{\partial t} = \frac{\partial}{\partial x} \lambda \frac{\partial T}{\partial x} + g(T_e - T) \cdot \tag{5}$$

Here the index "*e*" refers to the free electron population, g is the electron-lattice coupling factor, and all other parameters as in Eq. (1). To determine the laser energy term, it is necessary to calculate the dynamics of free electron generation. Here we consider one-photon ionization with the cross section σ_1 and avalanche ionization with the coefficient α_{av} as described in [16,17], taking into account that a-Si band gap E_g is 1.6 eV. The corresponding rate equation reads as

$$\frac{\partial n_e}{dt} = \sigma_1 \frac{I(x,t)}{\hbar\omega} + \alpha_{av} n_e - \frac{n_e}{\tau_0 + 1/C n_e n_i} \cdot \tag{6}$$

Here we consider relatively low fluences when $n_e << n_{at}$ with n_{at} to be the atomic density of unexcited a-Si. The last term of Eq. (6) represents free electron recombination with accounting for plasma screening at high excitations [16,18]. Knowing the free electron density, the source term in Eq. (6) can be defined as

$$\Sigma(x,t) = (\hbar\omega - E_g) \frac{\sigma_1 I(x,t)}{\hbar\omega} - E_g \alpha_{av} n_e + \frac{E_g n_e}{\tau_0 + 1/C n_e n_i} - \frac{3}{2} k_B T_e \frac{\partial n_e}{\partial t} \cdot \tag{7}$$

The laser intensity attenuation toward the material depth accounts only for free electron generation:

$$\frac{\partial I(x,t)}{\partial x} = \sigma_1 I(x,t) \cdot \tag{8}$$

Note that in this study we disregard the free electron absorption, assuming that one-photon absorption by valence electrons excited to the conduction band is dominating at green light excitation. Further details, including free electron parameters (heat capacity and thermal conductivity) can be found in [16,17].

4. Results

This section is divided into four parts according to the major results: 1) Sample stack and disk capture method, 2) Material modification and heat-affected layer, 3) Crystallinity and material composition, and 4) Laser-induced spatiotemporal temperature fields and removal mechanisms depending on pulse duration.

4.1. Sample stack and disk capture method

For the analysis of the influence of pulse durations on the laser lift-off process, we investigated the irradiated sample stack as well as the ablated material. Before starting the sample irradiation and material collection, the ablation thresholds for the different laser pulse durations were determined by Liu-method [5]. Referring to the different selective processing ranges, the laser fluence was adjusted near the lower limit above the particular ablation thresholds to avoid melting or ablation of the substrate layers.

For the capturing, we positioned a carbon pad (C-pad) at a distance of ~1 mm behind the thin film sample stack to collect fragments of the ablated material. A schematic setup of the irradiated sample stack and the C-pad which collects the ablated Si disks is illustrated in the left of Fig. 1. Depending on pulse duration and laser fluence, the collected thin film material pieces differ in size and morphology. In addition, in the case of too high fluences, the fracture of the layer occurs not only along the crater edges but also the strain at the crater center can exceed a critical value and lead to higher fragmentation [2,6]. Two SEM images of a fs ablated, collected thin film disk (a) and of an AZO crater after fs irradiation (b) are shown in Fig. 1. The center of the AZO crater and the thin film disk were selected for the preparation of TEM lamella and following TEM investigations, which are reasonable for the deposited Pt protection bases in the center of the disk. Such investigations have also been done for ns- and ps-pulses.

4.2. Material modifications and heat-affected layer

The ablation behavior mentioned above infers that a shortening of pulse duration can limit the stress on the lift-off material to prevent fracture in several individual parts. For a deeper understanding of the pulse duration dependence we measured the effective optical penetration depths [7] by examining structural properties of the laser crater and the lift-off material.

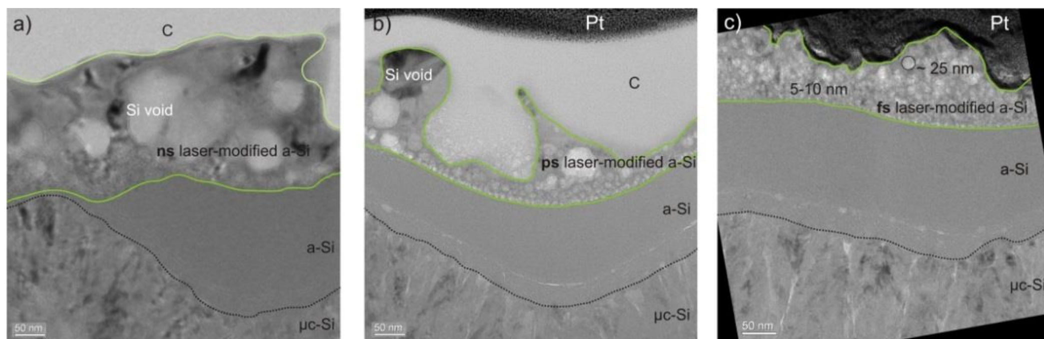

Fig. 2. TEM images of the cross sectional (a) ns-, (b) ps-, and (c) fs-laser-ablated Si thin film stack.

Figure 2 shows cross-sectional TEM images of (a) ns-, (b) ps-, and (b) fs-laser-ablated thin film disks. In the upper part of the images, the Pt protection base (ps, fs) and/or an additionally deposited carbon layer are seen which were needed to avoid electric sample charging during preparation (ns, ps). In all cases, the laser-modified regions are seen below the protection layers. These regions (marked by green lines) represent the effective optical penetration depth and the HAZ within the a-Si material. The thickness of the laser-modified layer was determined by the comparison of the thicknesses of an untreated a-Si layer (~250 nm, not shown) with the laser unaffected a-Si part underneath the modified a-Si region as indicated in Fig. 2. In ultrashort regimes, thickness measurements along the TEM lamella (ps and fs) reveal nearly the same average values for the unaffected region of <150 nm> for ps and <170 nm> for fs. Comparing with the reference a-Si

thickness (~250 nm), we conclude that ultrashort laser pulses affect layers of approximately 100 nm (ps) and 80 nm (fs) thicknesses. For the ns-pulses, thickness measurements along the TEM lamella reveal higher differences and more fluctuations between 50 and 250 nm (mainly around the spot centre). The morphology of the modified layers shows different structural phases, i. e. granular crystalline phases next to the unaffected a-Si interface followed by silicon voids on top of the modified region. Such voids indicate that evaporation process is involved during the laser lift-off. Qualitatively, we found a higher number of voids of larger dimension inside the ns and ps sample compared to the fs results.

4.3. Crystallinity and material composition

For evaluating the selectivity of the lift-off processes, the energy dispersive x-ray (EDX) analysis was performed in TEM measurements of the interface region to distinguish AZO and Si material phases. Inside the laser craters we found residual components of the respectively other material; Si on the crater bottom. Within the ablated material, only a negligible Zn amount was detected. Again, providing pulses in the fs regime leads to lower amount of residuals inside the laser groove and therefore a more accurate ablation selectivity. Raman measurements on the ablated disk indicate a phase change during laser-induced melting and ablation. Figure 3(a) shows the spectra of a reference a-Si (grey curve) and µc-Si layer (brown curve) compared to measurements of the ns-, ps- and fs-ablated material on laser-modified side.

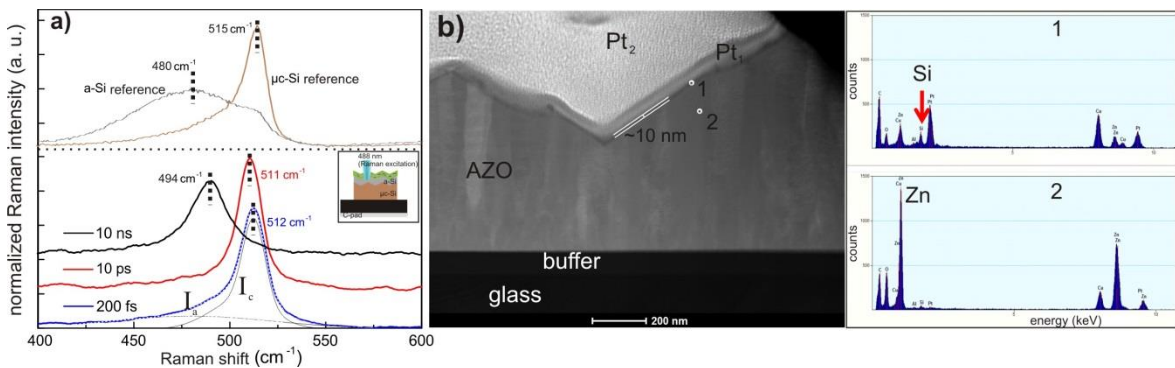

Fig. 3. a) Raman spectra of a-Si (grey) and µc-Si (brown) reference samples and of ns-, ps- and fs-ablated disk material with laser-modified side up, respectively; b) STEM cross section image of the opened fs-laser crater (top) and corresponding EDX spectra regarding to the indicated points 1 and 2.

Ultrashort (ps, fs) laser-modified area reveals a spectrum comparable to the Raman signal of µc-Si films (brown curve) with a strong band around 510-520 cm^{-1}. The band can be assigned to crystalline Si and so-called 'defect' c-Si phases inside the thin film lattice structure [8, 9]. The 'defect' c-Si component is usually assigned to crystallites with sizes lower than 10 nm [10]. Granular structures in this dimension range can be observed in both TEM-pictures of Fig. 2 on the junction between laser modification area and non-modified a-Si. In addition, the broad Raman bands connected to the amorphous phases of reference a-Si (grey curve) disappear almost completely in the spectra of the ultrashort (ps, fs) laser-modified a-Si layer. For the ns laser-modified a-Si layer, a narrowing and a peak position shift to 494 cm^{-1} were detected. A detailed study on this topic is in progress and will be presented in a forthcoming publication. Nevertheless, Raman results clearly indicate a phase change from amorphous to crystalline structure during confined laser ablation process.

Figure 3(b) shows a STEM cross section image of the opened fs-laser crater after Si ablation (left) and the corresponding EDX spectra indicated by points 1 and 2 (right). The STEM was operated in dark-field mode in

which crystalline sample regions appear brighter than amorphous parts similar to the buffer, glass and the thin unknown layer between Pt_1 and AZO. First EDX measurements reveal that this ~10 nm thick layer consists of Si (Fig. 3b). Hence, after ultrashort laser lift-off the AZO crater surface is not completely free of local Si residuals. The second EDX measurement provides a reference for the AZO substrate and the spectra show a strong Zn signal with no content of silicon inside the layer. In general, we detected more silicon residuals and, especially for ns processing, Si droplet formation (nm range) on the AZO crater surface.

4.4. Laser-induced spatiotemporal temperature fields and removal mechanisms depending on pulse duration

Ns laser pulses. All simulations have been performed for the film stack geometry as shown in Fig. 1. As laser-irradiation spot diameter is much larger compared to AZO/a-Si/μc-Si film stack, modeling has been performed for one-dimensional geometry. A special attention has been paid to modeling of action of ns laser pulses as the melting threshold of the AZO film can serve as a good test for the model. However, it was found that the direct application of the model as described in Section 3.1 highly overestimate the fluence which would be necessary to initiate the AZO melting. Figure 4 shows the spatiotemporal evolution of the temperature in the irradiated multilayer sample.

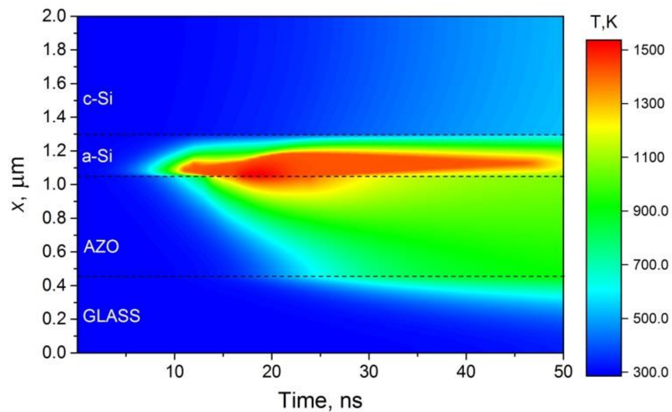

Fig. 4. Spatiotemporal evolution of the temperature of laser-heated multilayer sample at peak laser fluence of 0.3 J/cm^2. Laser pulse of 10-ns duration (FWHM) is propagating from the bottom to the top. Dashed lines indicate the interfaces between materials which are assumed to be smooth.

The maximum temperature of the sample is found to be ~1520 K that is enough for melting of a-Si but well below the melting point of AZO. As the AZO thermal conductivity is higher as compared to a-Si, it is seen that the heat is rapidly spreading through this film with almost stopping at the AZO-glass interface. Due to the low thermal conductivity of a-Si, the heat is slowly conducted to the a-Si/μc-Si interface and, after reached this boundary, it immediately spreads in μc-Si whose thermal conductivity is almost two orders of magnitude higher than that of a-Si. As a whole, the heat is mostly kept within a-Si film implying relatively high stresses in solidified hot layer which can be the reason of silicon film removal through mechanical ejection, similar to [15]. However, disagreement with the experiment on the AZO melting threshold requires a further analysis.

First, we note that, upon melting, silicon is considerably compacting that can result in detachment between AZO and a-Si film as shown schematically in Fig. 5(b). As molten silicon is viscous, it can create liquid bridges with AZO upon detachment. After detachment, a-Si layer will absorb incoming radiation without sharing heat with the AZO film. In such a case, a-Si will be heated to much higher temperatures than shown

in Fig. 4. With higher heating, liquid silicon as well as underlying solid silicon will expand, that can result in the back attachment to the AZO film. If Si melt is heated above the melting point of AZO, the latter can melt upon contacting as shown in Fig. 5(c). Finally, upon spreading the heat across a-Si/μc-Si stack and associated decrease in Si strength, silicon can be mechanically ejected from the sample as shown in Fig. 5(d). During this second detachment stage, viscous bridges can be formed again between the two molten surfaces, silicon and AZO, thus producing nanoparticles on their breakage (Fig. 5(d)).

To verify this scenario, the simulations have been performed under following assumption. As soon as the melting temperature is reached in a-Si, the boundary conditions at the interface between a-Si and AZO are changed from (3) to the reflection condition in both films ($\partial T/\partial x = 0$). After reaching 2250 K (chosen arbitrary and can be refined with accounting for the linear expansion coefficients), the boundary condition is again returned to the expression (3), assuming back attachment between molten Si and AZO.

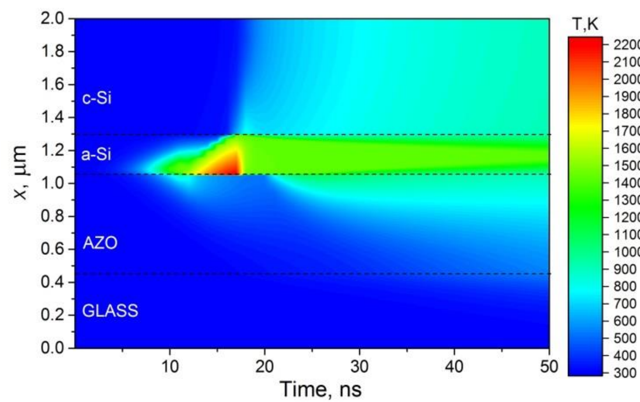

Fig. 5. Schematic representation of AZO melting scenario followed by stress-induced silicon removal. (a) Initial configuration of the film stack with the laser-heated region in a-Si. (b) Detachment of molten Si from AZO film due to a-Si compaction upon melting. Due to viscosity, liquid bridges can be organized. (c) Further heating of liquid silicon and underlying solid silicon results in Si expansion and back attachment to the AZO film. If the temperature of liquid silicon exceeds the melting point of AZO, the latter can melt at the contact zone. (d) Thermally expending a-Si/μc-Si films experience stresses, resulting in the mechanically driven lift-off from the film stack. Upon detachment of films, AZO and Si nanoparticles can be formed due to breakage of viscous bridges schematically shown in (b).

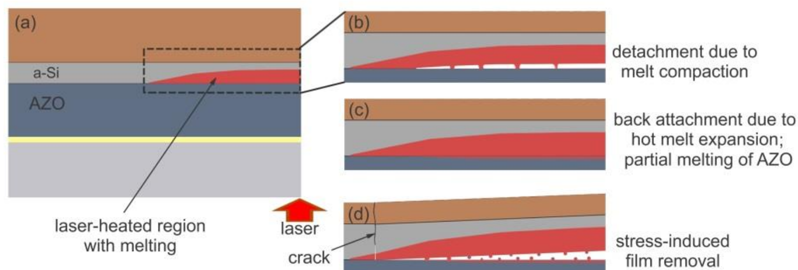

Fig. 6. Spatiotemporal evolution of the temperature of laser-heated multilayer sample at peak laser fluence of 0.34 J/cm^2 under the assumption of a transient detachment of a-Si film from AZO due to a-Si compaction upon melting. All other conditions as for Fig. 4.

The result of such simulation for 0.34 J/cm^2 is shown in Fig. 6 (simulations for 0.3 J/cm^2 did not yield in reaching the AZO melting temperature). Under assumption of transient detachment for only ~3.5 ns, the

dynamics of the sample heating is strongly changed. First, T_m of AZO is slightly exceeded in the adjacent liquid silicon layer, resulting in melting of a very thin but non-zero AZO layer. Second, much more heat has been directed toward μc-Si layer that should result in a considerable decrease of silicon strength and, hence, facilitate the lift-off of the heated a-Si/μc-Si layer from the sample.

Ps and fs laser pulses. At ultrashort laser pulses, the absorbed heat is strongly confined within a-Si layer at the picosecond timescale, thus resulting in (1) much lower melting threshold and (2) generation of high stresses due to large temperature gradients [19]. The temperature distribution across AZO/a-Si interface and in a-Si film is presented in Fig. 7 at 23 ps after the laser pulse maximum (pulse duration of 10 ps, laser fluence of 0.04 J/cm^2). By the dashed double-sided arrow, the molten layer of silicon is shown which is ~40 nm at this time moment and can be 10-20 nm wider for later moments. However, the melting threshold of a-Si film in simulations is ~0.031 J/cm^2, that is app. 25% smaller than in experiments. At 200-fs laser pulses, the model gives even larger discrepancy with experiment (~0.05 J/cm^2 vs. 0.07 J/cm^2 in experiment). This could be explained by the fact that we disregard the change of optical properties of a-Si upon free electron generation. However, the maximum free electron density remains subcritical for both ps and fs pulses near the melting threshold (~3×10^{20} cm^{-3} and ~8×10^{20} cm^{-3} respectively) that cannot induce substantial reflectivity change. More plausible explanation can be in material properties (both AZO and silicon) which are changing with temperature while here they are considered constant.

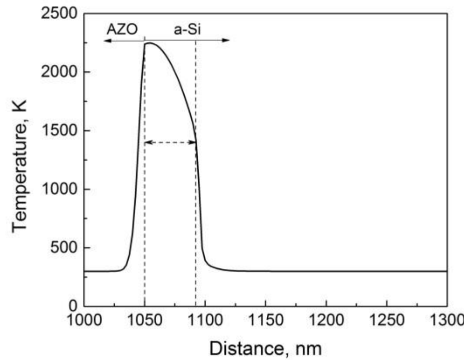

Fig. 7. The temperature profile across AZO/a-Si interface and in a-Si film for 10-ps laser pulse irradiation of the sample in Fig. 1. a-Si film 250 nm wide is located between 1050 and 1300 nm. Laser fluence is 0.04 J/cm^2, laser pulse is centered at 15 ps, distribution is given at time moment of 38 ps. The molten silicon layer is shown by the dashed double-sided arrow.

5. Conclusion

The results of this work clearly indicate that ultrashort laser pulse processing can be used for layer-selective thin film lift-off techniques in a typical glass/TCO/Si layer stack. Microstructural material investigations show a significant reduction of HAZ by changing from ns to ps and fs pulse durations. Thus, ablation efficiency and selectivity of fs- and ps-lift-off thin film processing in comparison to thermal ablation by ns pulses is strongly increased. Differences in layer modifications and ablation threshold in the ultrashort regime (ps, fs) were found, providing insight into the time-dependency of laser-material-interaction processes as well as compared to ns processing. Simulations based on the thermal and two-temperature models have enable to reveal interesting features of the laser heating process. One of them is detachment of a-Si from AZO upon its melting that explains observation of AZO melting at ns laser pulses. It was found theoretically that even a very short detachment between two layers during irradiation redirects heat flux toward silicon that should result in stronger modification of Si layers in ns irradiation regimes. For fs pulses,

very strong confinement of the absorbed energy in a-Si layer is found, in accordance with the experiments. Although quantitative agreement between modelling and experiment was not achieved, simulations support the experimental studies with a valuable qualitative insight.

Acknowledgements

The authors gratefully acknowledge the financial support by the German Ministry of Education and Research in the project 'MechSi' with the contract No. 03IPT607X. We also would like to thank Maren Kasischke and Prof. Evgeny Gurevich of Ruhr-University Bochum, Applied Laser Technology, for helping to perform the picosecond laser experiments. N.M.B. acknowledges the financial support of the European Regional Development Fund and the state budget of the Czech Republic (project BIATRI: CZ.02.1.01/0.0/0.0/15_003/0000445) and by the Ministry of Education, Youth and Sports (Programs NPU I - project no. LO1602, and Large Infrastructures for Research, Experimental Development and Innovations - projects no. LM2015086).

References

[1] G. Heise, M. Domke, J. Konrad, S. Sarrach, J. Sotrop & H. P. Huber, "Laser lift-off initiated by direct induced ablation of different metal thin films with ultra-short laser pulses", Journal of Physics D: Applied Physics, 45, 315303, 2012.

[2] S. Krause, P.-T. Miclea, F. Steudel, S. Schweizer, and G. Seifert, "Precise micro-structuring of indium-tin oxide thin films on glass by selective femtosecond laser ablation", EPJ Photovoltaics 4, 40601 (2013).

[3] D. Canteli, I. Torres, M. Domke, C. Molpeceres, J. Carabe, J. J. Gandia, G. Heise & H. P. Huber, "Picosecond-laser structuring of amorphous-silicon thin-film solar modules", Applied Physics A, Springer Berlin Heidelberg, 112, 695-700, 2013.

[4] M. Domke, L. Nobile, S. Rapp, S. Eiselen, J. Sotrop, H. P. Huber & M. Schmidt, "Understanding Thin Film Laser Ablation: The Role of the Effective Penetration Depth and the Film Thickness", Physics Procedia, 56, 1007-1014, 2014.

[5] J. M. Liu, "Simple technique for measurements of pulsed Gaussian-beam spot sizes," Optics Letters, 7, 196, 1982.

[6] J. Sotrop, A. Kersch, M. Domke, G. Heise, and H. P. Huber, "Numerical simulation of ultrafast expansion as the driving mechanism for confined laser ablation with ultra-short laser pulses", Applied Physics A 113, 397–411, 2013.

[7] S. Xiao, B. Schöps, and A. Ostendorf, "Selective Ablation of Thin Films by Ultrashort Laser Pulses", Physics Procedia, 39, 594-602, 2012.

[8] M. Luysberg, P. Hapke, R. Carius, and F. Finger, "Structure and growth of hydrogenated microcrystalline silicon: Investigation by transmission electron microscopy and Raman spectroscopy of films grown at different plasma excitation frequencies", Philosophical Magazine A, 75, 31-47, 1997.

[9] M. N. Islam and S. Kumar, "Influence of crystallite size distribution on the micro-Raman analysis of porous Si", Applied Physics Letters, 78, 715-717, 2001.

[10] H. Xia, Y. L. He, L. C. Wang, W. Zhang, X. N. Liu, X. K. Zhang, D. Feng, and H. E. Jackson, "Phonon mode study of Si nanocrystals using micro-Raman spectroscopy", Journal of Applied Physics, 78, 6705-6708, 1995.

[11] N. M. Liao, W. Li, Y. D. Jiang, Y. J. Kuang, K. C. Qi, Z. M. Wu and S. B. Li. "Raman study of a-Si:H films deposited by PECVD at various silane temperatures before glow-discharge", Applied Physics A, 91, 349–352, 2008.

[12] P. Borowicz, W. Latek, M.and Rzodkiewicz, A. Łaszcz, A. Czerwinski and J. Ratajczak, "Deep-ultraviolet Raman investigation of silicon oxide: thin film on silicon substrate versus bulk material". Advances in Natural sciences: Nanoscience and Nanotechnology, 3, 0450033, 2012.

[13] J. Sotrop, M. Domke, A. Kersch, and H. P. Huber, "Simulation of melting volume in thin molybdenum films as a function of the laser pulse duration", Physics Procedia, 41, 520-523, 2013.

[14] N.M. Bulgakova, A.V. Bulgakov, and L.P. Babich, "Energy balance of pulsed laser ablation: Thermal model revised", Appl. Phys. A, 79, 1323-1326, 2004.

[15] J. Bovatsek, A. Tamhankar, R.S. Patel, N.M. Bulgakova, and J. Bonse, "Thin film removal mechanisms in ns-laser processing of photovoltaic materials", Thin Solid Films, 518, 2897-2904, 2010.

[16] N.M. Bulgakova, R. Stoian, A. Rosenfeld, I.V. Hertel, W. Marine, and E.E.B. Campbell, "A general continuum approach to describe fast electronic transport in pulsed laser irradiated materials: The problem of Coulomb explosion", Appl. Phys. A, 81, 345-356, 2005.

[17] H. M. Van Driel, "Kinetics of high-density plasmas generated in Si by 1.06– and 0.53-μm picosecond laser pulses", Phys. Rev. B, 35, 8166–8176, 1987.
[18] J. Bok, and M. Combescot, "Comment on the evidence for a selfconfined plasma in laser annealing", Phys. Rev. Lett., 47, 1564, 1981.
[19] M.V. Shugaev and N.M. Bulgakova, "Thermodynamic and stress analysis of laser-induced forward transfer of metals", Appl. Phys. A, 101, 103-109, 2010.